The chemistry of additives in damascene copper plating

P. M. Vereecken
R. A. Binstead
H. Deligianni
P. C. Andricacos

Copper plating baths used for forming integrated circuit interconnects typically contain three or four component additive mixtures which facilitate the superfilling of via holes and trench lines during damascene plating. Extensive study over the last two decades has provided researchers with an understanding of the underlying mechanisms. The role of cuprous intermediates in the copper deposition reaction has long been acknowledged, but it is not yet fully understood. In this paper we describe the results of an electrochemical study of the interaction of the organic additives used with copper and copper ions in solution. It is shown that cuprous intermediates near the copper surface affect the overpotential and the kinetics of plating. The additives regulate the presence of cuprous species on the surface; levelers and suppressors inhibit Cu^{+} formation, whereas accelerating additives enhance Cu^{+} formation. Acceleration by the bis(sodiumsulfopropyl) disulfide (SPS) additive results from accumulation of cuprous complexes near the surface. Adsorbed cuprous thiolate $[Cu(I)(S(CH_2)_3SO_3H)_{ad}]$ is formed through interaction of Cu^{+} ions and SPS rather than Cu^{2+} and mercaptopropane sulfonic acid (MPS).

Introduction

The introduction of copper as a silicon chip interconnect material in 1997 by IBM resulted in a major change in silicon chip manufacturing [1]. Replacement of the traditional vacuum-deposited aluminum-based interconnects with plated copper-based interconnects was made possible by the integration of a thin liner material which acts as a diffusion barrier between copper and the underlying silicon. Key to the process was the invention and development of the damascene copper electroplating process for on-chip metallization, which was conceived at IBM in the early 1990s. The development of the copper damascene process [1, 2] and the subsequent implementation of the copper-based interconnects had a considerable impact on the electrochemical community, with a renewed interest in the mechanism of copper electrodeposition and the role of the organic additives.

Copper-sulfate-based plating processes have been used for some time in the electronics industry for through-hole plating of printed circuit boards. It was found that similar processes could be used to fill micron and submicron inlaid features. The damascene copper plating process uses a thin copper seed which covers the complete wafer surface, including trench and via openings, and acts as the cathode for electroplating the copper. Small amounts of organic additives can increase the plating rate in features relative to the planar surface, when added in the proper concentrations. The observed differential plating kinetics are better known as superfilling, superconformal, or bottom-up plating. Typical copper-sulfate-based electroplating solutions contain small amounts of chloride ions, polyethers such as polyethylene glycol (PEG) and polypropylene glycol (PPG) as a suppressor additive, a sulfur-based organic molecule such as bis(sodiumsulfopropyl) disulfide (SPS) as an accelerator or brightening agent, and in most cases an aromatic nitrogen-based molecule or polymer [e.g., thiourea, benzotriazole (BTA), Janus Green B (JGB)] that acts as a leveling agent to produce mirrorlike plated surfaces. In

0018-8646/05/$5.00 © 2005 IBM

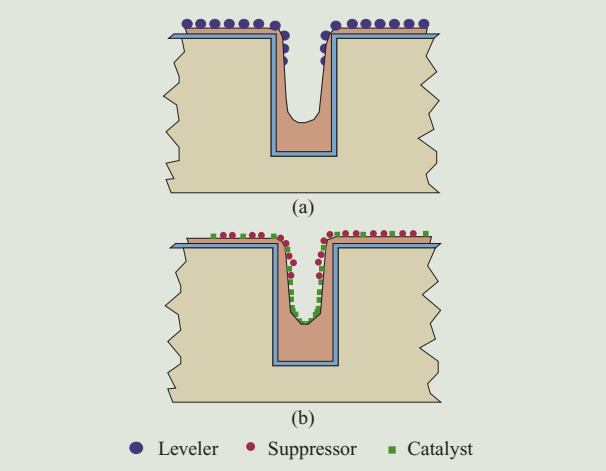

Figure 1

Schematics for superfilling mechanisms (a) with a strong adsorbing leveler for differential inhibition of plating in the field and at the mouth of a feature, and (b) with a catalyst or accelerator in the bottom of the feature for achieving differential acceleration.

combination, these additives can achieve accelerated, bottom-up electrodeposition of copper into submicron inlaid features, which permits void-free interconnect wiring in damascene structures.

Superfilling mechanisms

In recent years several models have been proposed in an attempt to describe the role of the organic additives in "superconformal" or "superfilling" plating. In general, differential plating rates inside and outside inlaid features can be obtained either by differential inhibition of the copper plating kinetics by diffusion–adsorption of strong adsorbing molecules such as levelers [2–5] or by differential acceleration of the plating kinetics by accumulation or generation of a catalyst inside the features [4, 6–9]. Schematics of both mechanisms are shown in **Figure 1.** Which of the two mechanisms prevails depends on the solution composition and the relative concentrations of the additives [4]. A system based on the action of a strong leveler additive such as JGB or BTA [10, 11] can be characterized approximately by the differential inhibition models, whereas systems with only SPS-type accelerators and PEG-type suppressors can be characterized more accurately by accelerator or catalyst models [12–15]. For three-component systems with suppressor, accelerator, and leveler, the dominance of a system depends on the relative concentrations of accelerator and leveler.

The leveler-dominated models are based on diffusion–adsorption leveling theories for single-component additives adapted to submicron damascene structures. Even though most copper plating baths contain multiple additives, experimental plated profiles from certain commercial baths can be well characterized by the differential inhibition model [4]. Differential inhibition is maintained through the diffusional flux of the leveler into the trench or via as a result of leveler consumption during plating. Characteristic of a leveler-dominated system are rounded profiles and relatively high impurity content in the plated copper because of leveler incorporation. Analysis by secondary ion mass spectroscopy (SIMS) has indeed shown higher C, O, S, and Cl impurities in copper films plated from leveler-dominated systems [4, 11]. Other systems investigated [4] showed poor correlation between plated profiles and modeling of differential inhibition. The authors explained this deviation by the possible accumulation of a catalyst inside the features [4].

In the case of the more recently used two-component (suppressor and accelerator) or three-component (with low leveler concentration) copper plating systems, it has been found that competition between the accelerator and the suppressor for adsorption sites can describe the superfilling of submicron features [6–9, 15]. The accumulation of the adsorbed catalyst due to a rapid change in surface area inside a trench or via is believed to be responsible for the observed bottom-up filling. The suppressor–chloride complex is replaced by the more stable adsorbed accelerator or catalyst complex [14]. West et al. [6] and Moffat et al. [7–9] have independently developed a mathematical description for the observed, fast bottom-up superfilling kinetics based on surface-enhanced accumulation of the accelerator. The curvature-enhanced acceleration accumulation (CEAC) mechanism was shown to be valid as well for silver plating [16, 17] and even for the chemical vapor deposition of copper [18]. The strength of both models is that they describe the extraneous plating or "bump" formation typically observed for the two-component systems. Also, the initial induction time typically seen before the onset of bottom-up fill and the typical square profiles can be simulated. The weakness of the CEAC model is that the electrochemical kinetic fitting parameters are determined from steady-state measurements, whereas the actual filling of features occurs during the dynamic initial transient period of plating.

It is evident that the change in surface area, and the accompanying change in surface-to-volume ratio inside trenches and vias, affects the coverage of adsorbed species on the copper surface. In addition, the depletion of cupric ions and additives, and the accumulation of reaction intermediates and products, are affected by the change in surface-to-volume ratio. The rapid change in the near-surface concentration should influence the electrodeposition kinetics as well as the heterogeneous adsorption/desorption reactions at the surface. In this paper we investigate the role of cuprous intermediates and their effect on copper electrodeposition kinetics.

Electrochemical and chemical interactions at the Cu/electrolyte interface

Table 1 shows a list of possible reactions at a copper surface in a copper sulfate plating bath containing typical additives. Five groups of reactions can be distinguished: copper comproportionation reactions, redox reactions involving SPS, surface adsorption reactions, exchange reactions, and complexation reactions. Metallic copper, cupric (Cu^{2+}) and cuprous (Cu^{+}) ions interact with one another through reaction {1}, which is known as the copper comproportionation (when shifted to the right) or copper disproportionation (when shifted to the left) reaction, with the following equilibrium constant[1] [19]:

$$K_{eq,Cu} = [Cu^{+}]^2/[Cu^{2+}] = 6.0 \times 10^{-7}\text{M}. \quad (1)$$

Free or uncomplexed cuprous ions are unstable in solution and readily react with dissolved oxygen. As a result, the copper sulfate plating bath contains only trace amounts of cuprous ions. When copper metal such as the copper seed on a wafer is introduced into the copper plating bath, cuprous ions are formed near the copper/electrolyte interface in order to facilitate the achievement of equilibrium for reaction {1}. For typical acid copper sulfate plating baths with 0.25 M to 0.5 M $CuSO_4$, according to Equation (1), about 0.4 millimolar (mM) to 0.6 mM of cuprous ions exist at the copper surface under open-circuit conditions. Since cuprous ions are oxidized by dissolved oxygen, equilibrium is not reached under ambient conditions. When a complexing agent such as chloride is added, a stable cuprous complex such as cuprous chloride can be formed (reaction {2}). For small Cl^{-} concentrations, an insoluble CuCl film is formed on the surface [19]. Also, MPS (mercaptopropane sulfonic acid) may act as a complexant forming Cu(I)thiolate species (reaction {3}) [20].

Reduction–oxidation reaction {4} shows interaction between SPS as the oxidant and Cu^{+} as the reductant. Depending on the relative concentrations of MPS and Cu^{+}, redox reactions {5} and {6} are obtained [21, 22].

Adsorption reaction {7} is the result of combining reactions {1} and {5} and shows the direct interaction of SPS with copper metal. Reaction {7} represents the chemical equivalent for the accelerator adsorption on the copper surface. Note, however, that this reaction may be slow or nonexistent without the occurrence of the comproportionation reaction {1}. The adsorption of the suppressor polymer is generally believed to be mediated through a CuCl film on the surface, as shown in reaction {8} [23–25].

Once the adsorbed species are formed on the surface, they may still interact with the solution bulk, and ligands can thus be exchanged, as shown in reactions {9} and {10}. The displacement of the suppressor–chloride complex by cuprous thiolate in reaction {10} is the chemical equivalent of the suppressor/accelerator competitive adsorption [14]. When the local surface concentration of chloride ions, MPS molecules, or SPS molecules changes because of the depletion or accumulation in a deep trench or via, exchange reactions may change the surface coverage of the adsorbed species. Also, the chemical equilibrium of the adsorption reaction

Table 1 Reactions at the copper/electrolyte interface in copper sulfate plating baths containing Cl^{-}, SPS [bis(sulfopropyl)disulfide: $S(CH_2)_3SO_3H)_2$] or MPS [mercaptopropane sulfonic acid: $HS(CH_2)_3SO_3H$] as accelerator and a polyether suppressor molecule [$H((CH_2)_xO)_yOH$]. The deprotonated MPS thiol group is indicated as "thiolate" in the formula.

Copper comproportionation reactions

{1} $Cu + Cu^{2+} \rightleftharpoons 2Cu^{+}$

{2} $Cu + Cu^{2+} + 2Cl^{-} \rightleftharpoons 2CuCl_{ad}$

{3} $Cu + Cu^{2+} + 2MPS \rightleftharpoons 2Cu(thiolate)_{ad} + 2H^{+}$

Redox reactions involving SPS

{4} $2Cu^{+} + SPS + 2H^{+} \rightleftharpoons 2Cu^{2+} + 2MPS$

{5} $4Cu^{+} + SPS \rightleftharpoons 2Cu^{2+} + 2Cu(I)(thiolate)_{ad}$

{6} $2Cu^{2+} + 4MPS \rightleftharpoons 2Cu(I)(thiolate)_{ad} + SPS + 4H^{+}$

Surface adsorption reactions

{7} $2Cu_s + SPS \rightleftharpoons 2Cu(I)(thiolate)_{ad}$

{8} $nCuCl_{ad} + HO((CH_2)_xO)_yH \rightleftharpoons \lfloor HO((CH_2)_xOCuCl)_n\ ((CH_2)_xO)_{y-n}H \rfloor_{ad}$

Exchange reactions

{9} $CuCl_{ad} + MPS \rightleftharpoons Cu(I)(thiolate)_{ad} + Cl^{-} + H^{+}$

{10} $\lfloor HO((CH_2)_xOCuCl)_n\ ((CH_2)_xO)_{y-n}H \rfloor_{ad} + nMPS \rightleftharpoons HO((CH_2)_xO)_yH + nCl^{-} + nCu(I)(thiolate)_{ad}$

Complexation reactions

{11} $Cu^{+} + Cl^{-} \rightleftharpoons CuCl_{ad}$

{12} $CuCl_{ad} + Cl^{-} \rightleftharpoons CuCl_2^{-}$

{13} $CuCl_{ad} + MPS \rightleftharpoons CuCl(thiolate)^{-} + H^{+}$

{14} $Cu^{+} + MPS \rightleftharpoons Cu(I)(thiolate)_{ad} + H^{+}$

{15} $Cu^{+} + SPS \rightleftharpoons Cu(I)(SPS) + H^{+}$

{16} $Cu(I)(thiolate)_{ad} + MPS \rightleftharpoons Cu(I)(thiolate)_2^{-} + H^{+}$

{17} $Cu(I)(thiolate)_{ad} + Cl^{-} \rightleftharpoons Cu(thiolate)Cl^{-}$

{18} $4Cu(I)(thiolate)_{ad} + Cu^{2+} \rightleftharpoons Cu[Cu(I)(thiolate)]_4^{2+}$

{19} $Cu(I)(thiolate)_{ad} + Cu^{+} \rightleftharpoons Cu(I)(thiolate)Cu(I) + H^{+}$

[1] Calculated from the standard redox potentials for half-reactions {20} and {21} in Table 1 according to $\ln K_{eq,Cu} = (F/RT)\,[U^0(Cu^{2+}, Cu^{+}) - U^0(Cu^{+}, Cu)]$.

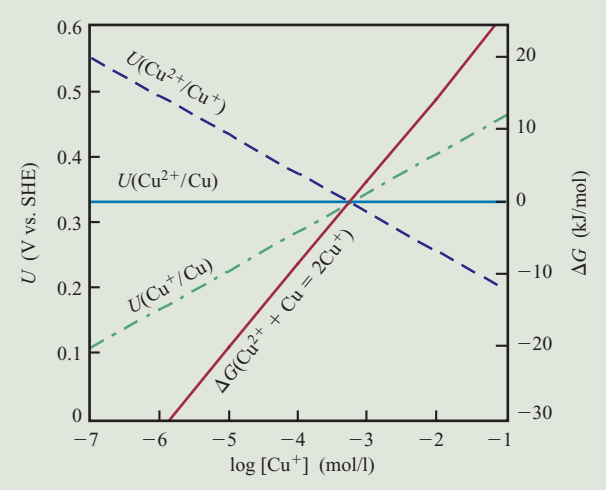

Figure 2

Nernst equilibrium potentials $U(Cu^{2+}, Cu^{+})$, $U(Cu^{+}, Cu)$, and $U(Cu^{2+}, Cu)$, and Gibbs free energy ΔG for the comproportionation reaction ($Cu + Cu^{2+} \rightleftharpoons 2Cu^{+}$), as a function of Cu^{+} concentration in a solution containing 0.55 M Cu^{2+}.

may shift because of the depletion of the reagents near the surface. For example, the depletion of chloride causes dissolution of the adsorbed CuCl, since the equilibrium is shifted toward free Cu^{+} and Cl^{-} (reverse reaction {11}). The same applies to the MPS (reactions {14} through {16}). In addition, higher complexation reactions may be responsible for the dissolution of adsorbed species, as shown for reactions {12}, {13}, and {16} through {19}.

Acceleration by cuprous ion complexes

Comproportionation reaction at the open-circuit state

The electrochemical copper deposition from cupric sulfate solutions proceeds through a stepwise reduction mechanism with the formation of cuprous ion as an intermediate, as shown in reactions {20} through {22} in **Table 2.** The standard redox potential $U^{0}(Cu^{2+}, Cu)$ for the copper deposition reaction {22} is the average of the standard redox potentials $U^{0}(Cu^{2+}, Cu^{+})$ and $U^{0}(Cu^{+}, Cu)$ for the half-cell reactions {20} and {21}, respectively. Under standard conditions (298 K, $a = 1$ M), the cuprous ion is more noble than the cupric ion, and the formation of cuprous ions is the rate-determining step. However, the concentration of cuprous ions in solution is typically very small; hence, the Nernst potentials for reactions {20} and {21} shift relative positions, as shown in **Figure 2.** For this reason the electrochemical reduction of Cu^{2+} to Cu^{+} can be observed at platinum electrodes before the onset of copper deposition (see the section on cuprous thiolate formation and Figures 8 and 9, shown later [26]). The combination of reaction {20} with the reverse reaction {21} results in the comproportionation reaction {1}. The Gibbs free energy, ΔG_{Cu}, for reaction {1} is given by the difference in Nernst potentials for reactions {20} and {21} in accordance with

$$\Delta G_{Cu} = F[U(Cu^{+}, Cu) - U(Cu^{2+}, Cu^{+})]. \quad (2)$$

It is shown in Figure 2 as a function of cuprous ion concentration for 0.55-M $CuSO_4$ solutions. Thermodynamic equilibrium ($\Delta G = 0$) is reached when the cuprous ion concentration $[Cu^{+}]_{eq} = 0.6$ mM. At this concentration, the Nernst potentials for reactions {20} and {21} become equal to the Nernst or equilibrium potential for the copper deposition reaction {22}:

$$U_{eq,Cu} = U^{0}(Cu^{2+}, Cu) + \frac{RT}{2F}\ln[Cu^{2+}]_{b}, \quad (3)$$

$$U_{eq,Cu} = U^{0}(Cu^{2+}, Cu^{+}) + \frac{RT}{F}\ln\frac{[Cu^{2+}]}{[Cu^{+}]_{eq}}, \quad (4)$$

$$U_{eq,Cu} = U^{0}(Cu^{+}, Cu) + \frac{RT}{F}\ln[Cu^{+}]_{eq}, \quad (5)$$

Table 2 Electrochemical half-cell reactions in copper sulfate plating baths containing Cl^{-}, SPS [bis(sulfopropyl)disulfide: $S(CH_2)_3SO_3H)_2$] or MPS [mercaptopropane sulfonic acid: $HS(CH_2)_3SO_3H$] as accelerator, and a polyether suppressor [$H((CH_2)_xO)_yOH$].

{20}	$Cu^{2+} + e^{-} \rightleftharpoons Cu^{+}$	$U^{0}(Cu^{2+}, Cu^{+}) = 0.153$ V vs. SHE
{21}	$Cu^{+} + e^{-} \rightleftharpoons Cu$	$U^{0}(Cu^{+}, Cu) = 0.521$ V vs. SHE
{22}	$Cu^{2+} + 2e^{-} \rightleftharpoons Cu$	$U^{0}(Cu^{2+}, Cu) = 0.337$ V vs. SHE
{23}	$Cu^{2+} + Cl^{-} + e^{-} \rightleftharpoons CuCl_{ad}$	$U^{0}(Cu^{2+}, CuCl) = 0.538$ V vs. SHE
{24}	$CuCl_{ad} + e^{-} \rightleftharpoons Cu + Cl^{-}$	$U^{0}(CuCl, Cu) = 0.137$ V vs. SHE
{25}	$Cu^{2+} + MPS + e^{-} \rightleftharpoons Cu(I)(thiolate)_{ad} + H^{+}$	
{26}	$Cu(I)(thiolate)_{ad} + H^{+} + e^{-} \rightleftharpoons Cu + MPS$	
{27}	$SPS + 2H^{+} + 2e^{-} \rightleftharpoons 2MPS$	

or 0.33 V vs. the standard hydrogen electrode (SHE) in a 0.55-M $CuSO_4$ solution. Note that combination of Equations (4) and (5) results in the equilibrium constant $K_{eq,Cu}$ in Equation (1). Substitution of Equation (1) in Equation (3) gives Equation (5), with $U^0(Cu^+, Cu)$ a function of $U^0(Cu^{2+}, Cu)$ and $K_{Cu,eq}$. In most cases the average cuprous concentration in the solution bulk is much lower than the equilibrium concentration, or $\Delta G_{Cu} < 0$, and the copper comproportionation reaction {1} is spontaneous (see Figure 2). As a result, the copper surface is not at equilibrium. Copper dissolves at a rate sufficient to maintain the near-surface cuprous concentration close to the equilibrium concentration. The measured open-circuit potential is therefore different from the calculated equilibrium potential. For example, the measured open-circuit potential for an aqueous 0.55-M $CuSO_4$ in a 0.45-M H_2SO_4 solution was found to be 0.27 V (SHE) or 60 mV more negative than the equilibrium value. According to Equation (2), $U(Cu^+, Cu) < U(Cu^{2+}, Cu^+)$ when $\Delta G_{Cu} < 0$. Therefore, the measured open-circuit potential is determined by $U(Cu^+, Cu)$ rather than by $U(Cu^{2+}, Cu)$ or by the cuprous concentration near the surface.

Effect of Cu^+ on copper deposition overpotential

A technique well suited to study the formation of cuprous intermediates is the rotating ring–disk electrode technique [27–29]. A fraction of the cuprous intermediates (determined by the collection efficiency N_0 of the ring–disk electrode) formed at the Cu disk are swept to a Pt ring, where they are oxidized quantitatively to Cu^{2+} when the ring is set at a potential >0.75 V (SHE) [>0.1 V vs. the $Hg/Hg_2SO_4/K_2SO_{4,sat}$ saturated mercury sulfate electrode (SMSE)]. **Figure 3** shows a current–potential curve for a rotating Cu-disk–Pt-ring electrode. The disk potential was scanned from the open-circuit state to −0.5 V (SMSE) and back; the ring was held at 0.25 V (SMSE). At the open-circuit potential (zero current at disk), a ring current was measured because of the dissolution of copper at the disk (comproportionation reaction {1}). After undergoing an initial small peak, the ring current decreased as the copper deposition current increased and reached its lower limit around −0.5 V, when the copper deposition current was about 20 mA/cm^2. In the reverse scan, chemical dissolution of copper through the comproportionation reaction {1} started again around −0.45 V (copper deposition current of 10 mA/cm^2) and reached a plateau when the open-circuit potential was reached. Even though these partial currents for cuprous formation were small and negligible with respect to the copper deposition reaction, the observation indicates that cuprous species are present near the surface at current densities typically used in the damascene process (2–15 mA/cm^2). In the potential region, where cuprous ions are detected at the ring, a current peak was seen in the forward (negative) potential scan at the copper disk. In the reverse scan (from a cuprous-depleted surface), a peak was no longer observed.[2] The excess copper deposition current in the forward scan (difference between forward and reverse current) is also plotted as a function of potential in Figure 3. It appears that the excess current varied with the ring current or was dependent on the near-surface concentration of cuprous ions.

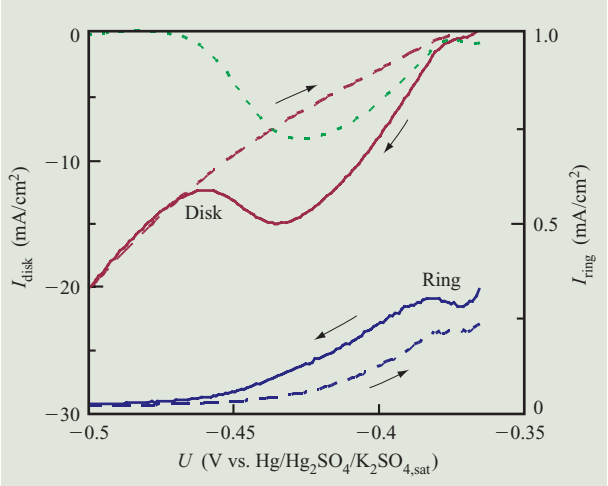

Figure 3

Current–potential curve for a rotating Cu-disk–Pt-ring electrode in 0.55 M $CuSO_4$ + 0.45 M H_2SO_4 (500 rpm). The potential of the Cu disk was scanned from open-circuit potential to −0.5 V (forward scan, solid curve) and back (reverse scan, dashed curve) at 10 mV/s. The potential of the Pt ring was held at 0.25 V, permitting detection of Cu^+ intermediates via the oxidation reaction: $Cu^+ \rightarrow Cu^{2+} + e^-$. The difference between the current in the forward and reverse scan (excess current, $I_{forw} - I_{rev}$) is also shown (dotted green curve).

Figure 4 shows the ring current associated with cuprous ion formation during plating [part (a)], together with the copper potential during galvanostatic (constant-current) deposition [part (b)]. For applied current densities smaller than 5 mA/cm^2, a relatively large concentration of cuprous ions was present at all times during deposition. For copper deposition current densities between 5 and 20 mA/cm^2, an initial current plateau was observed at the ring, which then relaxed to a steady-state value after about 40 s for 5 mA/cm^2 to 2 s for 20 mA/cm^2. At even higher applied current densities, the ring current immediately dropped to its low steady-state value. The measured potential in Figure 4(b) shows a transient which tracks the corresponding ring current very well. (Note

[2] A closer look revealed a small increase in disk current also in the reverse scan at the onset of the ring current.

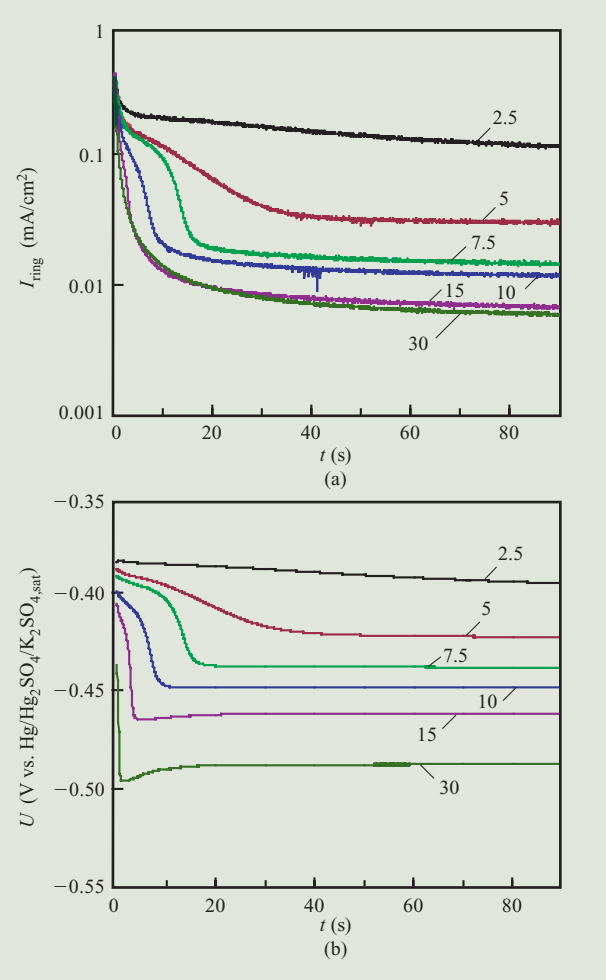

Figure 4

Ring current (a) and Cu potential (b) during galvanostatic copper deposition on a rotating Cu-disk–Pt-ring electrode in 0.55 M $CuSO_4$ + 0.45 M H_2SO_4 (at 500 rpm). The deposition current density (mA/cm^2) is indicated for each curve. The Pt ring was maintained at 0.25 V for detection of Cu^+.

that the observed correlation is between the logarithm of the ring current and the potential, in accordance with the Nernst equation.) The deposition potential was more positive when a higher ring current was measured or when the cuprous ion surface concentration was high. The deposition potential became constant when the cuprous ion formation reached steady state, and the shortest transients were seen for the highest applied copper deposition currents. The peak observed in the forward scan of the cyclic voltammogram (dynamic measurement) in Figure 3 follows directly from the time dependence of the potential and cuprous ion surface concentration of Figure 4. In the forward scan, the non-steady-state condition led to higher current densities corresponding to the more positive potentials and the cuprous-rich surface at small times during the galvanostatic experiments; the reverse scan represented the more negative steady-state potentials and the lower steady-state cuprous ion surface concentration conditions.

From the above discussion it is evident that the plating overpotential and the local current density depend on the local concentration of cuprous ions near the surface. So far we have considered planar electrode surfaces and additive-free solutions. The transient behavior, as shown in Figure 4, may be different in trench and via cavities compared with adjacent planar regions. The cuprous intermediates may be retained longer in cavities (because of slow out-diffusion or depletion of O_2) than in a planar field area, which slows down the transient because the potential profile is linked to the cuprous profile (see Figure 4). Hence, in this case, for the same applied potential, the current density and thus the copper deposition rate (corresponding to the peak of the forward scan of Figure 3) would be higher than at the planar field area (corresponding to the current in the reverse scan of Figure 3). In addition, since the cuprous ion surface concentration determines the local overpotential and plating rate, it is important to understand the effect of the plating additives on the formation of cuprous species. This is discussed next.

Additives and cuprous intermediate species

Typical cuprous species that are found on a copper surface in copper plating baths with additives are cuprous chloride ($CuCl_{ad}$) and cuprous thiolate [$Cu(I)(SCH_2CH_2CH_2SO_3H)_{ad}$ or $Cu(I)(thiolate)_{ad}$]. Both have been reported to have a small acceleration effect at moderate current densities in the absence of other additives [19, 30, 31]. **Figure 5** shows the effect of the different copper plating additives on the copper deposition current and on the ring current for cuprous ion formation. In all cases, a current peak, similar to that obtained for the additive-free solution, was seen during the forward scan at the copper disk. This indicated that in the presence of additives, the deposition potential and deposition rate continue to be determined by the cuprous near-surface concentration.

The addition of chloride resulted in an increase in the current with respect to the additive-free solution starting at small overpotentials [Figure 5(a)]. Note that chloride inhibited the excess current, seen for additive-free solutions, at very small overpotentials because of the formation of an insoluble CuCl film. When only an accelerator was added, an increase in the deposition current was observed at overpotentials at which cuprous ions are formed; this was similar to the behavior of the excess current in an additive-free solution [Figure 5(b)]. The area under the excess current increased with the time

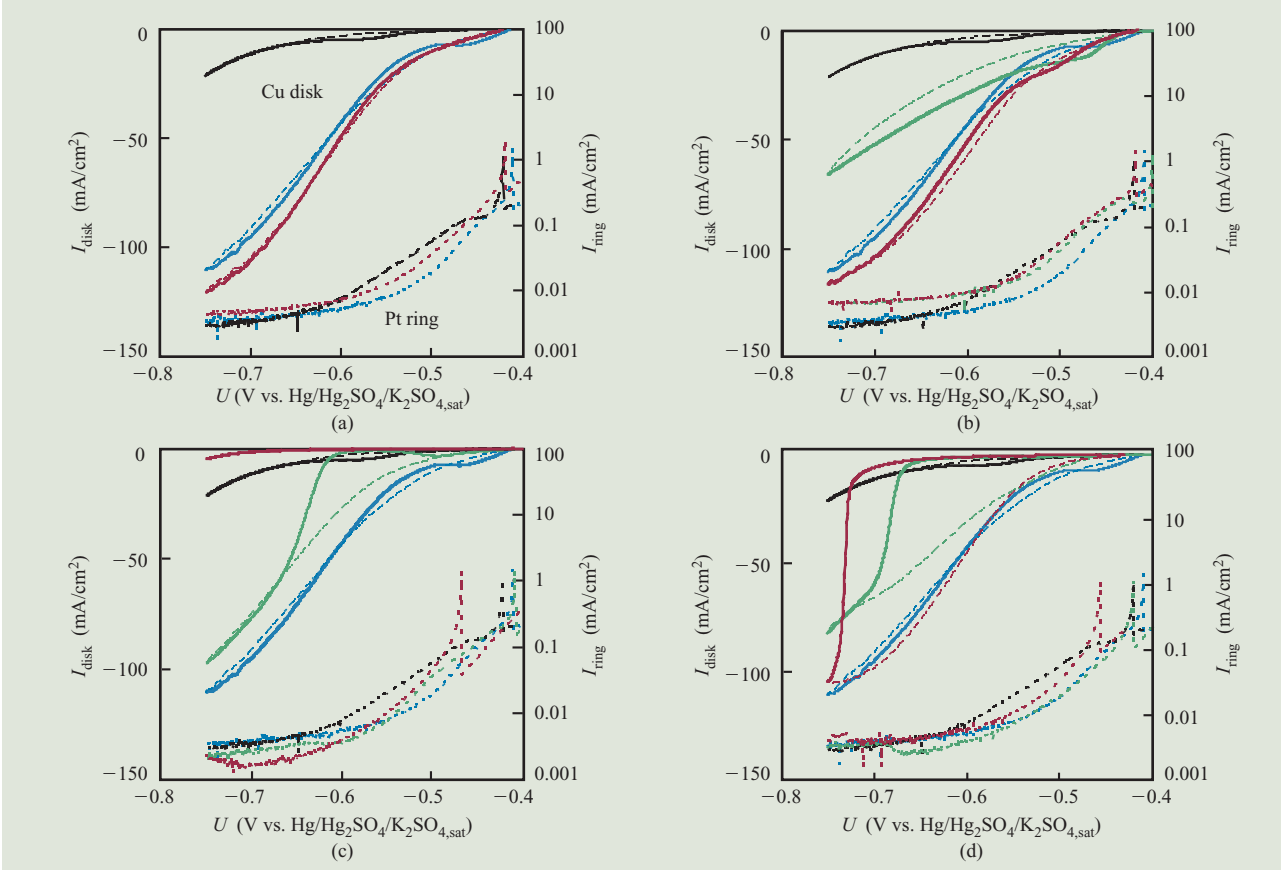

Figure 5

Current–potential curves for a rotating Cu-disk–Pt-ring electrode in 0.28 M $CuSO_4$ + 10 vol.% H_2SO_4 with and without additives, at 500 rpm and 10 mV/s. The ring was held at 0.5 V for detection of Cu(I) intermediates while the disk potential was scanned. The additives used were 50 mg/l Cl^-, 18 ml/l Shipley B2001 Brightener as accelerator, 25 ml/l Shipley C2001 Carrier as suppressor, and 3 ml/l Shipley L2001 Leveler as leveler. [Rohm and Haas Electronic Materials L.L.C., 455 Forest Street, Marlborough, MA 01752 (formerly Shipley Corporation L.L.C.).] Parts (a), (b), (c), and (d) compare results obtained for an additive-free solution (blue curve) and a solution containing all four additives (black curve) with those obtained via (a) chloride only (red); (b) accelerator only (green) and accelerator plus Cl^- (red); (c) suppressor only (green) and suppressor plus Cl^- (red) and (d) leveler only (green) and leveler plus Cl^- (red). The Cu potential was scanned from open circuit to −0.75 V (forward scan, solid curves) and back (reverse scan, dashed curves). For the ring current on Pt, only the forward scan is shown (dotted curves).

that the copper electrode was kept in solution before the start of the potential scan. At very large times, a brownish deposit could even be observed at the surface. A cuprous thiolate film which grew over time was most probably formed through the interaction of Cu^+ with SPS (reaction {5} in Table 1), since copper comproportionation is the only reaction in an open-circuit condition. The formation of adsorbed thiol layers is well known for self-assembled monolayers on noble metals such as Au and Ag, and also for Cu. Adsorption of a thiol (RSH) is mediated through oxidation of the metal (M) forming a stable RS–M surface layer [32, 33]. When disulfides are involved, the disulfide bond must be reduced before the thiol can adsorb. In the case of copper, Cu^+ is available both as the complexing metal ion and as a reductant for SPS.

For potentials negative of the peak in the ring current, the deposition current in the solution with SPS only became smaller than in the additive-free solution (about 60% of the additive-free current at −0.75 V). The adsorbed cuprous thiolate film seemed to inhibit the copper deposition reaction when no Cu^+ was formed near the copper surface. When both accelerator and Cl^- were present, the current–voltage curve showed acceleration at low overpotentials (similar to the accelerator-only case) and at high overpotentials (similar to the Cl^--only case). The acceleration at high overpotentials indicated that $CuCl_{ad}$ was preferentially formed over Cu(I)(thiolate)$_{ad}$.

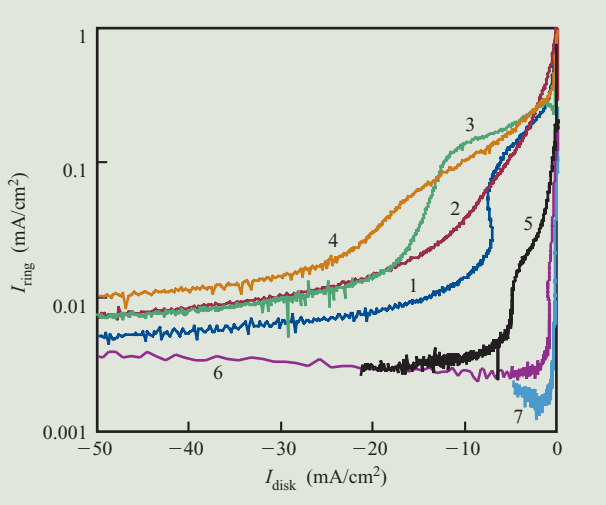

Figure 6

Ring current as a function of disk current in the forward scan for the current–potential curves at the rotating Cu-disk–Pt-ring electrode of Figure 5 (at 500 rpm and 10 mV/s) in 0.28 M $CuSO_4$ + 10 vol.% H_2SO_4 with and without additives. The additives used were 50 mg/l Cl^-, 18 ml/l Shipley B2001 Brightener as accelerator, 25 ml/l Shipley C2001 Carrier as suppressor, and 3 ml/l Shipley L2001 Leveler as leveler. Curve 1, additive-free solution; Curve 2, with Cl^- only; Curve 3, with accelerator only; Curve 4, with accelerator plus Cl^-; Curve 5, solution with all four additives; Curve 6, with leveler only; Curve 7, with suppressor plus Cl^-.

The kinetically fast formation of CuCl and subsequent adsorption of the suppressor compared with slow displacement by the accelerator has been reported by Teerlinck [14].

When only a suppressor or leveler was added to the solution, strong inhibition of the copper deposition was observed up to a certain potential [Figures 5(c) and 5(d), respectively]. At more negative potentials, the current increased rapidly because of desorption or breakdown of the suppressor or leveler from the surface. Inhibition was more effective for the leveler than for the suppressor even at a low leveler concentration. The addition of chloride resulted in a strong increase in inhibition for both the leveler and suppressor. In the case of chloride plus suppressor, the copper deposition current was almost completely blocked (4% of the additive-free current at −0.75 V), a phenomenon well known in the literature and attributed to the formation of the strong cuprous–chloride–ether complex, as shown in reaction {8} [14, 23–25]. Note that the commercial suppressor and leveler additive solutions used in this study may have contained chloride, and thus trace amounts of chloride may have been present in the solutions with suppressor and leveler only. When all additives were present in the plating solution, the deposition current was still predominantly inhibited compared with the additive-free solution (about 20% of the additive-free current at −0.75 V). The presence of the accelerator caused a slight increase in the deposition current (depolarization) compared with the fully suppressed current–voltage curve of suppressor plus chloride only. The CuCl–suppressor complex is partly displaced by the cuprous thiolate adsorbate (reaction {10}), which has much lower inhibition characteristics or a net acceleration. From the relative currents for the solution with the full additive package compared with those with suppressor plus chloride and with accelerator only, for a planar electrode surface, the surface coverage was estimated to be 1/3 for $Cu(thiolate)_{ad}$ and 2/3 for the suppressor–chloride adsorbate.

The current–voltage curves for the ring current measured as a function of copper potential were remarkably similar for the different additive mixtures [Figures 5(a)–5(d)]. Hence, the potential range for Cu^+ formation appears to be determined predominantly by the copper potential; only the cuprous formation rate was slightly affected by the addition of chloride, accelerator, suppressor, or leveler. The ring currents were higher for solutions containing chloride and accelerator than for solutions containing suppressor and leveler. Note that the ring currents increased when the suppressor and leveler desorbed at strongly negative potentials. When plotted as a function of current density in **Figure 6,** a large difference was seen in the ring current for the different additives. Accelerating additives such as chloride and accelerator showed a very large cuprous presence up to large current densities, whereas plating inhibitors such as suppressor and leveler showed no cuprous species present even at low current densities. Polarizing additives such as suppressor and leveler limited the presence of cuprous ions at typical plating currents, whereas depolarizing additives such as chloride and especially accelerator enhanced the formation of cuprous species during plating.

The above observation is entirely consistent with the finding in the previous section that the copper deposition overpotential is linked to the cuprous ion surface concentration. Indeed, an additive that prevents formation of soluble Cu^+ species requires a much more negative overpotential for the same current in additive-free solutions and thus has a "polarizing" effect. On the other hand, an additive that promotes formation of soluble cuprous intermediates has a more positive overpotential for the same current density in additive-free solutions and thus has a "depolarizing" effect. Hence, a differential in polarizing and depolarizing additives results in a differential in the near-surface concentration of cuprous species, and, in view of the previous section, also a differential in local current density.

In summary thus far, we have determined that cuprous intermediates are largely responsible for the local current

density through linkage of the near-surface cuprous concentration and overpotential, and that plating additives can enhance or inhibit the current density or plating rate by regulating the formation of soluble cuprous intermediates. In the next section we investigate in more detail the mechanism of current enhancement by the SPS accelerator.

Cuprous thiolate formation

Adsorbed cuprous thiolate has been identified in the literature as the catalyst most likely to be responsible for the accelerated copper deposition during damascene plating [21, 22, 30]. In previous sections we have already shown that accelerated copper plating occurs only when cuprous ions and complexes are detected near the surface, and is enhanced by the presence of SPS accelerators. In this section we investigate the interaction between SPS and Cu^{+} in more detail.

Cuprous thiolate can be present as an adsorbate on the surface $[Cu(I)S(CH_2)_3SO_3H)_{ad}]$ or in solution as a higher complex form with excess MPS $[Cu(I)(S(CH_2)_3SO_3H)_2^-]$ [34], or with Cu^{2+} ions to form a violet $[Cu(II)[Cu(I)S(CH_2)_3SO_3H]_4]$ complex [20], or possibly as $Cu(I)S(CH_2)_3SO_3Cu(I)$, where both the thiol and sulfonate groups function as ligand for Cu^{+} (reaction {19}). Two different mechanisms for the formation of cuprous thiolate have been proposed in the literature. In the first, SPS is assumed to be electrochemically reduced to MPS (reaction {27}), which then reacts with cupric ions to a Cu(thiolate) complex according to reaction {6} [34–37]. In the second, the formation of a cuprous thiolate species is assumed to occur through redox reaction of SPS with Cu^{+}, as shown in reaction {5} [20–22]. Both mechanisms are based on the same redox reaction {4} between Cu^{+} and SPS. The ratio of MPS to Cu^{+} determines the shift of reaction {4} through complexation of the unstable cuprous ions. For the first mechanism (reaction {6}), the excess of MPS (formed through direct electrochemical reduction of SPS to MPS at the electrode surface) complexes the Cu^{+} formed through reaction of Cu^{2+} with MPS (reverse reaction {4}). For the second mechanism (reaction {5}), the relative excess of Cu^{+} formed through the comproportionation reaction {1} or the stepwise reduction reaction {20} reacts with SPS, forming MPS as a complexant for Cu^{+}. The lack of thermodynamic data on complexation reaction {14} and half reaction {27} makes it difficult to exclude one or the other without experimental evidence.

Redox reaction {6} can be easily demonstrated by a change in solution color from blue to yellow after a Cu^{2+} solution is mixed with MPS [35, 38, 39]. In [34] the logarithm of the equilibrium constant for reaction {6} was found to be 3.3. Calculation of the free enthalpy for reaction {6} based on this equilibrium constant shows that reaction {6} is spontaneous only when either the SPS and MPS concentrations are large and comparable to the cupric concentration, or the ratio of MPS to SPS is large (1,000× for micromolar concentrations of SPS). Hence, only if SPS were reduced at the surface under diffusion limitation (surface concentration of SPS close to zero and MPS twice the SPS bulk concentration) would a mechanism through reaction {6} be applicable. However, literature studies are ambiguous as to whether direct electrochemical reduction of SPS to MPS at the electrode surface occurs. Zhukauskaite and Malinauskas have claimed the existence of a reversible reduction wave for SPS at a Pt electrode positive from the copper deposition potential [35]. However, we were unable to detect electrochemical reduction of SPS from sulfuric acid solutions at Pt, glassy carbon (GC), or copper before the onset of hydrogen evolution [40]. Also, Healy et al. have reported the absence of a reduction wave for SPS in both the presence and absence of Cu^{2+} [21]. On a gold electrode we were able to measure a reduction wave for 10–50-millimolar solutions of SPS in 10-vol.% sulfuric acid at potentials negative of 0.14 V (SHE) [40], i.e., still in the range of copper deposition (see Figure 5). However, in the case of gold we were most likely examining the electrochemical reaction of SPS and Au(I)thiolate [32, 33].

Whereas the direct electrochemical reduction of SPS was found to be difficult, the electrochemical oxidation of SPS was rather straightforward. **Figure 7** shows a rotating ring–disk voltammogram for GC ring and disk electrodes in a 0.05-M SPS solution. The disk potential was scanned from the open-circuit state to −1.5 V, reversed to 1.1 V (SMSE) and back to the open-circuit state. An oxidation wave for SPS was observed at $U > 0.5$ V, and a diffusion-limited plateau was reached at 0.9 V. In the reverse scan, the disk current was slightly lower because of adsorption of the oxidation products. The GC ring was polarized at 0.9 V, a potential at which SPS was oxidized under diffusion limitation. Under these conditions, the consumption of SPS at the disk can be determined quantitatively [41]. When no SPS was consumed at the disk, the ring current was at its limiting value, $I_{ring,lim}$. When SPS was consumed at the disk, the ring current decreased because of the shielding effect of the disk. This operating condition of the rotating ring–disk electrode (RRDE) is known as the "shielding" mode; the partial disk current associated with SPS consumption, I_{cons}, can be obtained from the measured ring current via the expression

$$I_{cons} = \frac{(I_{ring,lim} - I_{ring})}{N_0}, \quad (6)$$

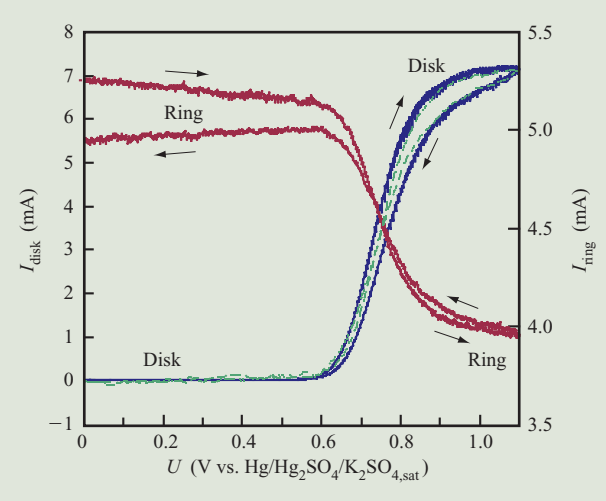

Figure 7

Current–potential curves for rotating glassy carbon (GC) disk and ring electrodes in 0.05 M SPS + 10 vol.% sulfuric acid. The GC-disk potential was scanned from the open-circuit state to −1.5 V, reversed to 1.1 V, and back to the open-circuit state (only positive potential range is shown). The GC ring was held at 0.9 V, a potential at which SPS is oxidized under diffusion limitation (1,000 rpm, 25 mV/s). The dashed curves show the SPS consumption current at the disk calculated from the ring current [Equation (6)].

with N_0 being the collection efficiency of the RRDE. The partial consumption current, I_{cons}, calculated from Equation (6) is also plotted in Figure 7. MPS and SPS showed a similar oxidation wave at the GC electrode, and both could be detected quantitatively at 0.9 V.

In order to verify the mechanism of SPS consumption and the formation of adsorbed or soluble cuprous thiolate complexes during copper deposition, we conducted a rotating ring–disk electrode study in copper sulfate solutions in which the ring was used to detect cuprous ions as well as SPS and MPS or its thiolate anion [$^{-}S(CH_2)_3SO_3H$]. A glassy carbon ring and a platinum disk were used. Glassy carbon was chosen as the material for the ring electrode since, in contrast to Pt or Au, it allowed the detection of SPS down to micromolar concentrations without excessive interference from surface adsorption. To minimize the change in collection efficiency due to slow adsorption of the oxidation products, a relatively fast scan rate was used. Distinguishing between the cuprous ion oxidation current and the SPS, MPS, or thiolate oxidation currents at the ring was possible because of the well-separated oxidation waves for Cu^+ (under diffusion limitation at 0.5 V) and SPS and MPS (under diffusion limitation at 0.9 V). When the ring was set at $U_{ring} = 0.5$ V, Cu^+ was detected in collection mode: i.e., an increase in ring current was seen when Cu^+ was formed at the disk. For the ring set at $U_{ring} = 0.9$ V, SPS was detected in the shielding mode (i.e., a decrease in ring current would be measured when SPS is consumed at the disk), and MPS or thiolate species were detected in the collection mode (i.e., an increase in ring current would be measured when thiolate species are formed at the disk). Note that the reduction of one SPS molecule leading to the formation of two MPS molecules at the disk would actually be detected as a net increase in ring current.

Figure 8 shows a typical current–potential curve for a Pt-disk–GC-ring electrode in copper sulfate solution with 500 μM SPS. The disk current showed copper deposition and stripping at the Pt electrode. The corresponding ring currents measured during subsequent scans with the GC ring at 0.5 V and 0.9 V are also shown in Figure 8. A sharp peak for the Cu^+ ring current was measured at the start of copper deposition for the rings at both 0.5 V and 0.9 V. Also, during the stripping of copper from the Pt electrode, Cu^+ was detected. When the Pt disk was swept to even more positive potentials ($U > 0.7$ V), the 0.9-V ring current decreased because of the oxidation of SPS at Pt. Note the similarity with the experiment of Figure 7.

Details of the disk currents in the positive potential region are shown in **Figure 9(a)**. The smaller current range of Figure 9(a) reveals the oxidation wave for SPS superimposed on the Pt oxidation wave at $U > 0.7$ V. The corresponding decrease of the 0.9-V ring current is also shown, in this case already corrected for the limiting current, $I_{ring,lim}$. The oxidation current on the Pt and the respective consumption current at the ring increased with increasing SPS concentration. Note that similar results were obtained for the 100-μM and 500-μM solutions, the former being within the concentration range used in typical damascene plating baths.

The small cathodic current peak around 0.0 V in Figure 9(a) corresponds to the underpotential deposition (UPD) of Cu on Pt. At the same potentials, a small decrease in the 0.9-V ring currents was also observed. For the ring at 0.5 V and for the solutions without additives, no such dip in current was observed. Hence, we infer that the SPS was adsorbed as soon as the first monolayer of copper was formed on the Pt disk. The charge under the dip in the curves was estimated to be 35 $\mu C/cm^2$, or 10 to 20 Cu atoms per adsorbed SPS molecule.

Details of the disk currents in the negative potential region are shown in **Figure 9(b)**. At low overpotentials [-0.44 V $< U < -0.6$ V (SMSE)], the copper deposition was faster in the solutions with SPS than in the additive-free solution. The opposite was true at high overpotentials [$U < -0.6$ V (SMSE)]. A similar observation was made for a Cu electrode in solutions with SPS only [Figure 5(b)]. Both the acceleration and inhibition effects of SPS were enhanced with increasing concentration. Acceleration of the copper deposition

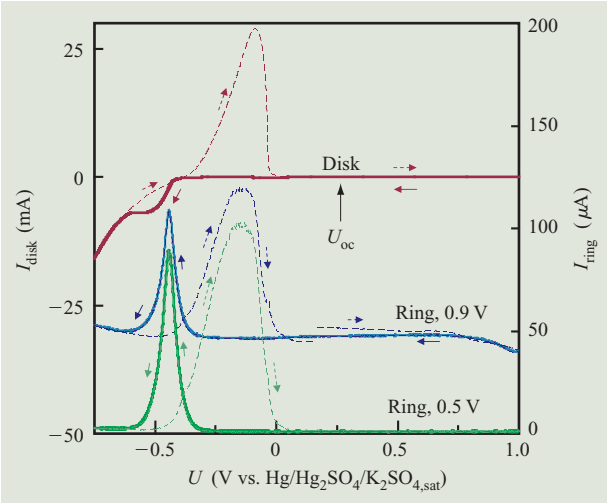

Figure 8

Current–potential curves for a rotating Pt-disk–GC-ring electrode (500 rpm) in 0.28 M $CuSO_4$ + 10 vol.% H_2SO_4 with 500 μM SPS, purged with nitrogen gas. The Pt disk was scanned from the open-circuit state to 1 V (positive scan, dashed curves), reversed to −0.8 V (negative scan, solid curves) and back to open-circuit potential U_{oc} (positive scan, dashed curves) at a relatively fast scan rate of 50 mV/s in order to minimize the adsorption of oxidation products at the ring. The ring currents were measured at 0.5 V and 0.9 V in two consecutive scans (with excellent reproducibility).

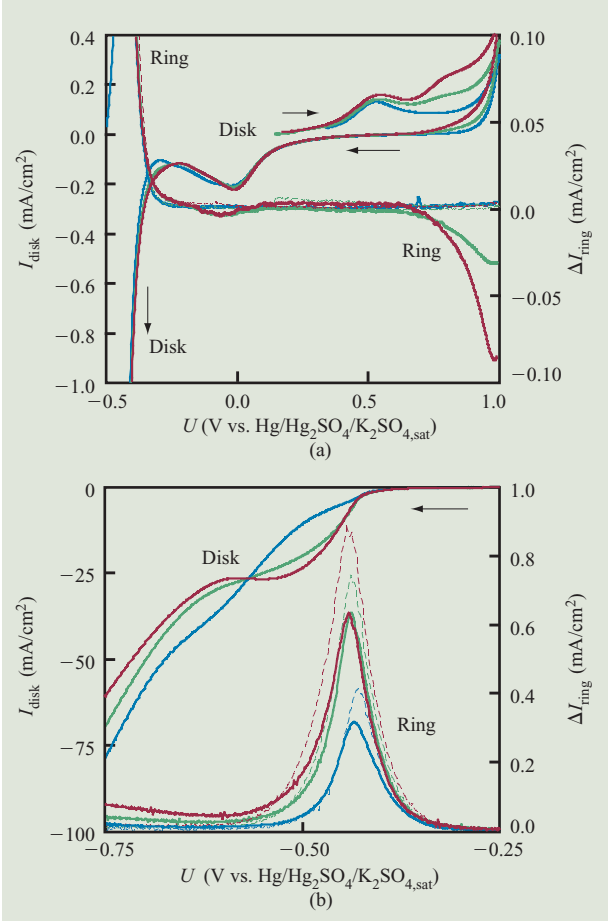

Figure 9

Current–potential curves for a rotating Pt-disk–GC-ring electrode (500 rpm) in 0.28 M $CuSO_4$ + 10 vol.% H_2SO_4 with 0 (blue), 100 μM (green), and 500 μM (red) SPS additive, purged with nitrogen gas (50 mV/s). The ring currents were measured at 0.5 V (dashed curve) and 0.9 V (solid curve) in two consecutive scans; the ring current at 0.9 V was corrected for the limiting current for SPS oxidation at the GC ring at zero disk current. (a) Detail of the positive potential scan for Pt from the open-circuit potential to 1 V and after reversal at the onset of copper deposition. (b) Detail of the negative potential scan for the copper deposition.

reaction was accompanied by strong Cu^+ formation, whereas no Cu^+ was detected when the deposition was inhibited, consistent with the cuprous–overpotential linkage described in previous sections. The onset of the excess deposition current corresponded to the maximum in the ring current at −0.44 V (SMSE). Note that the cuprous formation on Pt started at more positive potentials than the copper deposition potential because $U(Cu^{2+}, Cu^+)$ is more positive than $U(Cu^{2+}, Cu)$ (see Figure 2).

Two major observations could be made regarding the measured ring current peaks for Cu^+ at the start of the copper deposition. First, and most important, the peak current for the ring at 0.9 V was lower than that for the ring at 0.5 V in all cases, and the difference became more pronounced at higher SPS concentrations. A relative decrease in the 0.9-V ring current indicated a net consumption of SPS. This can be explained either by regular physical adsorption of the SPS on the copper or by adsorption of its reaction products (formation of two free MPS molecules per one SPS molecule would show up as a relative increase.[3] Since SPS consumption at the Cu surface was observed only during Cu^+ formation (and not at higher overpotentials), the adsorption reaction must involve Cu^+. Hence, we have indirect evidence for the formation of Cu(I)(thiolate)$_{ad}$ by the interaction of Cu^+ with SPS (reaction {5}).

Second, the ring current increased considerably with the addition of SPS to the solution for the rings at both 0.5 V and 0.9 V [Figure 9(b)]. A sharp increase in Cu^+ near the surface (which followed from the increase in the 0.5-V ring current) appears to indicate the formation of soluble stable cuprous complexes due to the presence of SPS in solution. The formation of the Cu(I)(thiolate)$_2^-$

[3]Both SPS and MPS are oxidized in a two-electron reaction. The ring at 0.9 V measures the sum of Cu^+ + SPS + MPS (or thiolate anion). A relative increase in the 0.9-V ring current compared with 0.5 V (Cu^+ only) indicates additional MPS. For example, the direct electrochemical reduction of one SPS (consumed) molecule to two MPS (collected) molecules would have a net oxidation current at 0.9 V.

complex (reaction {16}) is unlikely, since the extra thiolate anion would cause a relative increase in the 0.9-V ring current rather than the observed decrease (see Footnote 3). Another possible stable cuprous complex is $Cu(I)SPS^{+}$ [38], which would be undetectable by the ring at 0.9 V. An argument against this is that superfilling or acceleration is also found for "derivatized" substrates in plating solutions without SPS or accelerator added [13, 14]. This leaves us the possibility of a $Cu(I)(thiolate)Cu^{+}_{aq}$ complex. In this case, the preformed $Cu(I)(thiolate)_{ad}$ surface for derivatized substrates can still form stable cuprous complexes.

When the solutions were not purged with nitrogen, the ring currents for Cu^{+} were typically much lower because of the fast competitive oxidation of Cu^{+} by dissolved oxygen (not shown). Accordingly, the excess currents for accelerated copper deposition at low overpotentials were also lower in the ambient solutions. This observation supports the notion that the acceleration is controlled by the near-surface concentration of Cu^{+} and its complexes. The SPS accelerator merely enhances the formation of stable Cu^{+} complexes, which enhances the current density as described in previous sections. Dissolved oxygen, on the other hand, decreases the Cu^{+} concentration near the surface, thus slowing down the reaction. The role of oxygen in damascene plating may have been underestimated. Depletion of oxygen in trench and via cavities enhances the differential in cuprous concentration and hence the plating kinetics.

In summary, the rotating ring–disk experiments did not show any evidence for the direct electrochemical reduction of SPS to MPS. This observation excludes a catalytic mechanism whereby the adsorbed cuprous thiolate intermediary is formed through the interaction of Cu^{2+} with MPS. Evidence of considerable SPS consumption was found in the potential range of cuprous ion formation, which was correlated with the formation of $Cu(I)(thiolate)_{ad}$. In addition, the presence of SPS in the copper sulfate solutions was found to increase the amount of soluble cuprous complexes near the surface.

Differential plating kinetics

From our results, it is concluded that the near-surface concentration of cuprous ions, intermediates, or complexes is linked to the overpotential and thus the kinetics of copper electrodeposition. The depolarizing effect of rate-accelerating additives (Cl^{-} and SPS accelerator) and the polarizing effect of rate-inhibiting additives (suppressor and levelers) follow directly from this cuprous–overpotential linkage. Time-dependent differences in cuprous species inside trench and via cavities and at the planar field may then account for the differential plating kinetics responsible for superconformal plating or superfilling. Because of the cuprous-regulating properties of the plating additives, this concept does not contradict existing models based on physical adsorption and the time-dependent differential additive coverage in cavities and the field such as the curvature-enhanced accelerator coverage (CEAC) mechanism. In these models the copper deposition kinetics is determined by the surface coverage θ of accelerator or catalyst (and indirectly by suppressor coverage, $1 - \theta$), and the rapid change in surface coverage inside cavities accounts for the fast bottom-up plating kinetics [6–16]. The actual catalytic acceleration mechanism is of no concern in these models, since the kinetic parameters are obtained from electrochemical measurements. From our results, it follows that acceleration indeed occurs where $Cu(I)(thiolate)_{ad}$ is adsorbed at the surface. The increased copper deposition rate is the result of enhanced cuprous-complex formation at these adsorption sites, accounting for the so-called catalytic effect. In addition, a large differential in copper deposition rate is formed between $Cu(I)(thiolate)_{ad}$ sites and adsorbed suppressor–chloride sites, where cuprous formation is inhibited. A major advantage of this physical–chemical approach is that concentration changes due to in- and out-diffusion of reagents and products, together with other less obvious solution components, such as Cl^{-}, O_2, and oxidation byproducts, can also be accounted for. A disadvantage is the complexity of the mechanism and the need for sophisticated modeling [42]. However, the main contribution of the physical–chemical mechanism is that it provides an understanding of the underlying mechanisms.

Some discrepancies between the physical adsorption models and our physical–chemical mechanism have emerged. The physical adsorption models consider a surface layer of accelerator catalyst, whereas the physical–chemical mechanism considers a cuprous near-surface layer in coexistence with the actual adsorbed $Cu(I)(thiolate)_{ad}$ layer on the surface. The actual cuprous near-surface concentration determines the kinetics, whereas the $Cu(thiolate)_{ad}$ maintains the cuprous near-surface film, as is discussed later in more detail. This means that the increase in cuprous ion concentration, rather than the surface crowding of catalyst and subsequent increase in catalyst surface coverage (due to the decrease in cavity surface), is the major determining factor. The former is of course directly related to the latter, thus closely simulating the adsorbed catalyst layer assumption. However, the near-surface cuprous layer is also dependent on other external factors such as the cuprous consumption and diffusion of reagents and products. The diffusion may involve the out-diffusion of cuprous complexes as well as the in-diffusion of reagents

such as Cu^{2+}, SPS and MPS for formation, and O_2 for consumption (also direct electrochemical reduction accounts for consumption). In addition, surface coverage of the adsorbed suppressor–chloride complex is also affected by the concentration of species such as Cl^-, Cu^{2+}, and suppressor nearby[4] [43, 44]. In conclusion, the physical–chemical mechanism provides fine tuning of the physical adsorption models.

The physical–chemical mechanism presented in this paper also applies to the superfilling using derivatized copper surfaces on a semiconductor wafer [13, 14]. In this case, the copper surface is immersed first in a solution with only accelerator [13], or in a plating solution containing all additives [14], in order that a sub-monolayer of accelerator [13] or both accelerator and suppressor–chloride be adsorbed to the surface. The wafer is then brought into the copper plating solution without accelerator (only chloride and suppressor are present). The interaction of the SPS accelerator with copper during immersion (open-circuit) allows formation of cuprous thiolate on the surface. In the section on additives and cuprous intermediate species, we described an experiment in which the peak or excess current during the forward scan increased with time spent at the open-circuit state because of the formation of a thick cuprous thiolate film before a voltammogram was obtained. Superfilling with derivatized surfaces would then imply that Cu(I)thiolate$_{ad}$ is capable of maintaining an enhanced cuprous ion or complex formation near the surface, even without SPS present. A possibility would be the formation of a soluble $Cu(I)S(CH_3)_3SO_3Cu(I)$ complex. This complex can be formed directly through interaction of Cu(I)(thiolate)$_{ad}$ with free Cu^+ or indirectly through complexation with Cu^{2+}, forming $Cu(I)S(CH_3)_3SO_3Cu(II)$ as an intermediate. Stopped-flow experiments of the homogeneous reaction of Cu(II) and MPS have indeed shown that Cu(I)thiolate can serve as catalyst for the homogeneous reduction of Cu^{2+} [39]. Then the catalytic action could be the basis for the increase in Cu^+ detected in solution with SPS compared to solutions without SPS. In solutions with SPS, the Cu(I)(thiolate)$_{ad}$ film would be replenished continuously. However, when a thick enough thiolate film is formed by derivatizing the surface before plating, replenishment is not necessary. Note that the actual superfilling of submicron inlaid features requires only a few seconds, and even sub-monolayer coverage could be sufficient to maintain the near-surface cuprous concentration. Also, the increased cuprous ion formation at adsorbed Cu(I)(thiolate)$_{ad}$ sites does not necessarily imply the formation of complexes with MPS or SPS.

[4] J. G. Long, P. C. Searson, and P. M. Vereecken, "Electrochemical Impedance Spectroscopy Study of Suppressor–Chloride Complex Adsorption and Desorption on Copper Surfaces," in preparation.

Finally, we briefly discuss the action of the suppressor and leveler inhibiting species in copper plating baths. Adsorption and desorption of the suppressor–chloride complex on the copper surface is strongly dependent on the chloride ion concentration. At a certain potential, the suppressor or leveler desorbs from the surface [see for example Figure 5(d)]. Depending on the type of suppressor and the pH level, the critical potential of desorption shifts 60 to 120 mV positive per decade decrease in chloride ion concentration [14, 41]. Once the copper surface is free of suppressor, the accelerator forms a Cu(I)(thiolate)$_{ad}$ surface. The newly formed cuprous thiolate film hinders the formation of $CuCl_{ad}$ necessary for re-adsorption of the suppressor [14]. As a result, a strong hysteresis is observed for current–voltage curves extended past the desorption potential [6, 12]. Similarly, when copper grows out of a trench or via, the Cu(I)(thiolate)$_{ad}$ surface is not replaced by the suppressor–chloride complex. The thiolate-covered surface continues to accelerate plating because of the enhanced cuprous ion formation at the Cu(I)(thiolate)$_{ad}$ surface compared with the neighboring suppressed copper in the field areas. As a result, a "bump" is formed over the inlaid features in two-component systems. Nitrogen-based levelers, on the other hand, are capable of displacing the thiolate from the surface, and copper is inhibited as soon as it protrudes from a feature. As a result, relatively flat profiles are obtained in three-component systems that contain trace amounts of leveler. A diffusive flux which is maintained through consumption of leveler in the feature ensures leveler action only at the surface; interference with gap filling is minimal when the leveler concentration is low.

Conclusions

A correlation between the copper deposition potential and the near-surface concentration of cuprous ions at the copper electrode has been demonstrated through rotating ring–disk experiments. The "cuprous ion near-surface concentration–deposition potential" linkage causes copper deposition to be faster at cuprous-rich than at cuprous-poor surfaces for the same applied potential. This effect results in the small current peak observed in cyclic voltammograms at low overpotentials. The action of "polarizing" and "depolarizing" additives is explained respectively by the inhibition and acceleration of cuprous ion formation. The differential copper deposition rate in damascene plating is explained by the differential in cuprous ion complexes near adsorbed suppressor–chloride and adsorbed cuprous thiolate [$Cu(I)(S(CH_3)_3SO_3H)_{ad}$ or Cu(I)(thiolate)$_{ad}$] on copper. The so-called catalytic effect of the cuprous thiolate adsorbate follows from the enhanced formation of soluble cuprous complexes at these sites. Acceleration of

copper deposition occurs at low overpotentials, at which cuprous ions are formed. Adsorbed cuprous thiolate is formed through interaction of Cu^{+} ions and SPS rather than Cu^{2+} and MPS. Existing physical adsorption models and a proposed physical–chemical model are compared.

Acknowledgment

The authors thank John G. Long for assistance with many of the rotating disk electrode experiments during his internship at IBM in the summer of 2003.

References

1. D. Edelstein, J. Heidenreich, R. Goldblatt, W. Cote, C. Uzoh, N. Lustig, P. Roper, T. McDevitt, W. Motsiff, A. Simon, J. Dukovic, R. Wachnik, H. Rathore, R. Schulz, L. Su, S. Luce, and J. Slattery, "Full Copper Wiring in a Sub-0.25mm CMOS ULSI Technology," *Technical Digest, IEEE International Electron Devices Meeting*, 1997, p. 773.
2. P. C. Andricacos, C. Uzoh, J. O. Dukovic, J. Horkans, and H. Deligianni, "Damascene Copper Electroplating for Chip Interconnections," *IBM J. Res. & Dev.* **42**, 567–574 (1998).
3. A. C. West, "Theory of Filling High-Aspect Ratio Trenches and Vias in Presence of Additives," *J. Electrochem. Soc.* **147**, 227–232 (2000).
4. H. Deligianni, J. Horkans, K. Kwietniak, J. O. Dukovic, P. C. Andricacos, S. Boettcher, S.-C. Seo, P. Locke, A. Simon, S. Seymour, and S. Malhotra, "Model of Superfilling in Damascene Electroplating: Comparison of Experimental Feature Filling with Model Predictions," *Electrochemical Processing in ULSI Fabrication III*, P. C. Andricacos, P. C. Searson, C. Reidsema-Simpson, P. Allongue, J. L. Stickney, and G. M. Oleszek, Eds., PV 2000-8, Toronto, 2000, p. 145.
5. M. Georgiadou, D. Veyret, R. L. Sani, and R. C. Alkire, "Simulation of Shape Evolution During Electrodeposition of Copper in the Presence of Additive," *J. Electrochem. Soc.* **148**, C54–C58 (2001).
6. A. C. West, S. Mayer, and J. Reid, "A Superfilling Model that Predicts Bump Formation," *Electrochem. & Solid-State Lett.* **4**, C50–C53 (2001).
7. T. P. Moffat, D. Wheeler, W. H. Huber, and D. Josell, "Superconformal Electrodeposition of Copper," *Electrochem. & Solid-State Lett.* **4**, C26–C29 (2001).
8. D. Josell, D. Wheeler, W. H. Huber, J. E. Bonevich, and T. P. Moffat, "A Simple Equation for Predicting Superconformal Electrodeposition in Submicrometer Trenches," *J. Electrochem. Soc.* **148**, C767–C773 (2001).
9. D. Wheeler, D. Josell, and T. P. Moffat, "Modeling of Superconformal Electrodeposition Using the Level Set Method," *J. Electrochem. Soc.* **150**, C302–C310 (2003).
10. J. J. Kelly, C. Tian, and A. C. West, "Leveling and Microstructural Effects of Additives for Copper Electrodeposition," *J. Electrochem. Soc.* **146**, 2540–2545 (1999).
11. K.-C. Lin, J.-M. Shieh, S.-C. Chang, B.-T. Dai, C.-F. Chen, and M.-S. Feng, "Electroplating Copper in Sub-100nm Gaps by Additives with Low Consumption and Diffusion Ability," *J. Vac. Sci. Technol. B* **20**, 940–945 (2002).
12. T. P. Moffat, J. E. Bonevich, W. H. Huber, A. Stanishesky, D. R. Kelly, G. R. Stafford, and D. Josell, "Superconformal Electrodeposition of Copper in 500–90 nm Features," *J. Electrochem. Soc.* **147**, 4524–4535 (2000).
13. T. P. Moffat, D. Wheeler, C. Witt, and D. Josell, "Superconformal Electrodeposition Using Derivatized Substrates," *Electrochem. & Solid-State Lett.* **5**, C110–C112 (2002).
14. I. Teerlinck, "Electrochemical Copper Deposition in IC Manufacturing," Ph.D. Thesis, Universiteit Gent in collaboration with IMEC, Leuven, Belgium, 2002, Chapter 5.
15. Y. H. Im, M. O. Bloomfield, S. Sen, and T. S. Cale, "Modelling Pattern Density Dependent Bump Formation in Copper Electrochemical Deposition," *Electrochem. & Solid-State Lett.* **6**, C42–C46 (2003).
16. T. P. Moffat, B. Baker, D. Wheeler, J. E. Bonevich, M. Edelstein, D. R. Kelly, L. Gan, G. R. Stafford, P. J. Chen, W. F. Egelhoff, and D. Josell, "Superconformal Electrodeposition in Submicrometer Features," *J. Electrochem. Soc.* **149**, C423–C428 (2002).
17. B. C. Baker, M. Freeman, B. Melnick, D. Wheeler, D. Josell, and T. P. Moffat, "Superconformal Electrodeposition of Silver from a $KAG(CN)_2$-KCN-KSeCN Electrolyte," *J. Electrochem. Soc.* **150**, C61–C66 (2003).
18. D. Josell, Sibum Kim, D. Wheeler, T. P. Moffat, and Sung Gyu Pyo, "Interconnect Fabrication by Superconformal Iodine-Catalyzed Chemical Vapor Deposition of Copper," *J. Electrochem. Soc.* **150**, C368–C373 (2003).
19. D. M. Soares, S. Wasle, K. G. Weil, and K. Doblhofer, "Copper Ion Reduction Catalysed by Chloride Ions," *J. Electroanalyt. Chem.* **532**, 353–358 (2002).
20. L. Y. Valentelis, "Changes in the Near-Electrode Concentration of Cu^{+} Ions Under the Effect of Brighteners in Sulfate Electrolytes," *Protect. Met.* **32**, 38–41 (1996).
21. J. P. Healy, D. Pletcher, and M. Goodenough, "The Chemistry of the Additives in an Acid Copper Electroplating Bath, Part II. The Instability of 4,5-Dithiaoctane-1,8-Disulphonic Acid in the Bath on Open Circuit," *J. Electroanalyt. Chem.* **338**, 167–177 (1992).
22. J. P. Healy, D. Pletcher, and M. Goodenough, "The Chemistry of the Additives in an Acid Copper Electroplating Bath, Part III. The Mechanism of Brightening by 4,5-Dithiaoctane-1,8-Disulphonic Acid," *J. Electroanalyt. Chem.* **338**, 179–187 (1992).
23. J. P. Healy, D. Pletcher, and M. Goodenough, "The Chemistry of the Additives in an Acid Copper Electroplating Bath, Part I. Polyethylene Glycol and Chloride Ion," *J. Electroanalyt. Chem.* **338**, 155–165 (1992).
24. J. J. Kelly and A. C. West, "Copper Deposition in the Presence of Polyethylene Glycol I. Quartz Crystal Microbalance Study," *J. Electrochem. Soc.* **145**, 3472–3476 (1998).
25. V. D. Jovic and B. M. Jovic, "Copper Electrodeposition from a Copper Acid Bath in the Presence of PEG and NaCl," *J. Serbian Chem. Soc.* **66**, 935–952 (2001).
26. G. Fabricius, K. Kontturi, and G. Sundholm, "Influence of Thiourea and Thiourea Ageing on the Electrodeposition of Copper from Acid Sulfate Solutions Studied by the Ring-Disc Technique," *J. Appl. Electrochem.* **26**, 1179–1183 (1996).
27. G. W. Tindall and S. Bruckenstein, "A Ring-Disk Electrode Study of the Electrochemical Reduction of Copper (II) in 0.2M Sulfuric Acid on Platinum," and "A Ring-Disk Electrode Study of the Deposition and Stripping of Thin Copper Films at Platinum in Sulfuric Acid," *Analyt. Chem.* **40**, 1051–1054 and 1637–1640 (1968).
28. M. Yokoi, S. Konihi, and T. Hayashi, "Mechanism of the Electrodeposition and Dissolution of Copper in an Acid Copper Sulfate Bath: I. The Behavior of Intermediate, Cu^{+}," *Denki Kagaku* **51**, 310–316 (1983).
29. P. M. Vereecken, F. Vanden Kerchove, and W. P. Gomes, Electrochemical Behaviour of (100) GaAs in Copper(II)-Containing Solutions," *Electrochim. Acta* **41**, 95–107 (1996).
30. J. J. Kim, S.-K. Kim, and Y. S. Kim, "Catalytic Behavior of 3-Mercapto-1-Propane Sulfonic Acid on Cu Electrodeposition and Its Effect on Cu FIM Properties for CMOS Device Metallization," *J. Electroanalyt. Chem.* **542**, 61–66 (2003).
31. M. Yokoi, S. Konishi, and T. Hayashi, "Mechanism of the Electrodeposition and Dissolution of Copper in an Acid Copper Sulfate Bath IV. Acceleration Mechanism in Presence of Cl^{-} Ions," *Denki Kagaku* **51**, 460–464 (1983).
32. S. Wong and M. D. Porter, "Origin of the Multiple Voltammetric Desorption Waves of Long-Chain Alkenethiolate Monolayers Chemisorbed on Annealed Gold Electrodes," *J. Electroanalyt. Chem.* **485**, 135–143 (2000).

33. S. Chon and W. Paik, "Adsorption of Self-Assembling Sulfur Compounds Through Electrochemical Reactions: Effects of Potential, Acid and Oxidizing Agents," *Phys. Chem. Chem. Phys.* **3**, 3405–3410 (2001).
34. A. Survilla, S. Kanapeckaite, and R. Pauliukaite, "Polarographic Behaviour of Cu(II) Solutions Involving 3-Mercapto-1-Propanesulphonic Acid," *Chemija (Vilnius)* **1**, 21–26 (1998).
35. N. Zhukauskaite and A. Malinauskas, "Electrocatalysis by a Brightener in Copper Electrodeposition," translated from *Elektrokhimiya* **24**, 1691–1694 (1988).
36. N. A. Zhukauskaite and A. A. Malinauskas, "Mechanism of the Brightening Effect of the Disulfide of Dipropanedisulfacid in Acid Copper Plating Electrolytes," *Protect. Met.* **25**, 132–136 (1989).
37. E. Farndon, F. C. Walsh, and S. A. Campbell, *J. Appl. Electrochem.* **25**, 572 (1995).
38. A. Frank and A. J. Bard, "The Decomposition of the Sulfonate Additive Sulfopropyl Sulfonate in Acid Copper Electroplating Chemistries," *J. Electrochem. Soc.* **150**, C244–C250 (2003).
39. R. A. Binstead, R. Mikkola, and J. M. Calvert, "Fundamental Mechanism Controlling Copper Electrodeposition. The Roles of Organic and Inorganic Components in Promoting Superconformal Filling and Self-Leveling of Inlaid Submicron Interconnects," Abstract 189, Annual AIChE meeting, San Francisco, 2003; to be published in proceedings volume *Fundamental Challenges in Electrodeposition*.
40. P. M. Vereecken, H. Deligianni, K. T. Kwietniak, P. C. Andricacos, R. A. Binstead, J. Wu, R. Mikkola, and J. M. Calvert, "The Role of SPS in Damascene Copper Electroplating," 201st Meeting of The Electrochemical Society, Meeting Abstracts 2002-1, No. 517, 2002.
41. A. J. Bard and L. R. Faulkner, *Electrochemical Methods: Fundamentals and Applications*, Second Edition, John Wiley & Sons, Inc., New York, 2001, Chapter 9, p. 352.
42. T. O. Drews, F. Xue, X. Liu, H. Deligianni, P. M. Vereecken, E. I. Cooper, P. C. Andricacos, R. D. Braatz, and R. C. Alkire, "Parameter Estimation of a Copper Electrodeposition Additive Mechanism Using Data Obtained from a D-Optimal Experimental Design," Abstract 189b, Annual AIChE meeting, San Francisco, 2003; to be published in proceedings volume *Fundamental Challenges in Electrodeposition*.
43. M. Hayase, M. Taketani, K. Aizawa, T. Hatsuzawa, and K. Hayabusa, "Copper Bottom-up Deposition by Breakdown of PEG–Cl Inhibition," *Electrochem. & Solid-State Lett.* **5**, C99–C101 (2002).
44. M. Hayase, M. Taketani, T. Hatsuzawa, and K. Hayabusa, "Preferential Copper Electrodeposition at Submicrometer Trenches by Consumption of Halide Ion," *Electrochem. & Solid-State Lett.* **6**, C92–C95 (2003).

Received March 18, 2004; accepted for publication July 29, 2004; Internet publication December 7, 2004

Philippe M. Vereecken *IBM Research Division, Thomas J. Watson Research Center, P.O. Box 218, Yorktown Heights, New York 10598 (pvereeck@us.ibm.com).* Dr. Vereecken is a Research Staff Member in the Electrochemical Processes–Copper Plating Group in the Silicon Science and Process Technology Department at the Thomas J. Watson Research Center. He received a licentiate degree (M.Sc. equivalent) in chemistry and a Ph.D. degree in physical chemistry with specialization in semiconductor electrochemistry from the University of Ghent (Belgium) in 1993 and 1998, respectively. He studied the correlation between electrochemical metal deposition on III–V semiconductors and the properties of the obtained metal gates. Dr. Vereecken then spent three years as a postdoctoral associate in Professor P. C. Searson's group in the Department of Materials Science and Engineering at The Johns Hopkins University, studying finite size effects in electrochemically formed thin films and nanowires. He joined IBM in 2001 and has been working on electrochemical processes for fabricating copper interconnects for current and future silicon chip generations. Dr. Vereecken is an author and co-author of more than twenty scientific publications, one patent, and six patent applications. He is a member of The Electrochemical Society and the American Association for the Advancement of Science.

Robert A. Binstead *Rohm and Haas Electronic Materials L.L.C., 455 Forest Street, Marlborough, Massachusetts 01752 (rbinstead@rohmhaas.com).* Dr. Binstead joined Rohm and Haas Electronic Materials L.L.C. (formerly Shipley Corporation L.L.C.) in 2000 as a Senior Scientist for copper electrodeposition research and development. He received B.Sc. (Hons, 1975) and Ph.D. (1979) degrees in inorganic chemistry from Sydney University, Australia, where he studied the kinetics of electron-transfer and electronic spin state relaxation phenomena. This was followed by postdoctoral research at the University of North Carolina at Chapel Hill (with Prof. T. J. Meyer, 1979–1980), where he participated in kinetic isotope effect and photochemical studies of ruthenium polypyridine systems. He returned to Sydney University as a professional officer (with Prof. N. S. Hush, 1981–1984) to study the spectroscopy and electrochemistry of oxo-bridged metalloporphyrin and phthalocyanine oligomers. He emigrated to the U.S. in 1986, first working at the Naval Research Laboratory (1986–1989). He then returned to the University of North Carolina at Chapel Hill (1990–1997), where he undertook detailed mechanistic studies on transition metal oxidation catalysts. Dr. Binstead has published 27 scientific papers, holds three patents, and has developed commercial scientific software based on his research work at University of North Carolina at Chapel Hill. He is a member of the American Chemical Society and the Electrochemical Society.

Hariklia Deligianni *IBM Research Division, Thomas J. Watson Research Center, P.O. Box 218, Yorktown Heights, New York 10598 (lili@us.ibm.com).* Dr. Deligianni manages the Electrochemical Processes Group at the IBM Thomas J. Watson Research Center. She received a B.S. degree in chemical engineering from Aristotelion University, Thessaloniki, Greece, in 1982, and M.S. and Ph.D. degrees from the University of Illinois at Urbana–Champaign in 1986 and 1988, respectively. Since joining IBM in 1988, she has successfully introduced electrochemical processes into the solder-based C4 technology, playing a key role in developing the processes and transferring them to IBM manufacturing. As well as being a key participant in the study of the feasibility of copper metallization for on-chip interconnects, she later developed mathematical models for the design and operation of electrodeposition tools and process models of feature filling during copper electroplating for such interconnects. Throughout her 16 years at IBM, Dr. Deligianni has worked on diverse and interesting projects such as the integration of passives and MEMS for wireless communications. More recently,

her group has been working to develop electrochemical processes for fabrication of future CMOS logic chips. Dr. Deligianni has received an IBM Corporate Technical Excellence Award, an IBM Outstanding Innovation Award, and IBM Patent Awards. She holds ten patents and is an author of 40 publications in technical journals and conference proceedings. Dr. Deligianni is a member of the Executive Committee of the Electrodeposition Division of the Electrochemical Society, a member of the Electrochemical Society, a member of the American Institute of Chemical Engineers, and a member of IEEE.

Panayotis C. Andricacos *IBM Research Division, Thomas J. Watson Research Center, P.O. Box 218, Yorktown Heights, New York 10598 (ndricac@us.ibm.com)*. Dr. Andricacos, who passed away on November 21, 2004, was a manager in the Silicon Science and Process Technology Department at the IBM Thomas J. Watson Research Center. He received B.S., M.S., and doctoral degrees in chemical engineering from Columbia University, where he was also an adjunct associate professor. As a postdoctoral research associate at the Lawrence Berkeley Laboratories, he worked on fuel cells and on the application of ultrahigh-vacuum techniques to the study of electrochemical reactions. While at IBM, Dr. Andricacos worked on the application of electrochemical processes in storage, packaging, and C4 technologies; he played a pioneering role in the development of copper electroplating for semiconductor on-chip metallization. In 1993, he received the Research Award of the Electrodeposition Division, Electrochemical Society, for the development of novel techniques for the study of alloy electroplating.